Pre-flight calibration of LYRA, the solar VUV radiometer on board PROBA2

A. Benmoussa, I. E. Dammasch, Jean-François Hochedez, U. Schuhle, S. Koller, Y. Stockman, F. Scholze, M. J. Richter, U. Kroth, C. Laubis, et al.

A&A 508, 1085–1094 (2009)
DOI: 10.1051/0004-6361/200913089

Astronomy & Astrophysics

Pre-flight calibration of LYRA, the solar VUV radiometer on board PROBA2

A. BenMoussa[1,9], I. E. Dammasch[1], J.-F. Hochedez[1], U. Schühle[2], S. Koller[3], Y. Stockman[4], F. Scholze[5], M. Richter[5], U. Kroth[5], C. Laubis[5], M. Dominique[1], M. Kretzschmar[6], S. Mekaoui[7], S. Gissot[1], A. Theissen[2], B. Giordanengo[1], D. Bolsee[8], C. Hermans[8], D. Gillotay[8], J.-M. Defise[4], and W. Schmutz.[3]

[1] Royal Observatory of Belgium, SIDC, Circular Avenue 3, 1180 Brussels, Belgium
e-mail: ali.benmoussa@oma.be
[2] Max-Planck-Institut für Sonnensystemforschung, 37191 Katlenburg-Lindau, Germany
[3] Physikalisch-Meteorologisches Observatorium Davos – World Radiation Center, 7260 Davos Dorf, Switzerland
[4] Centre Spatial de Liège, Av. Pré Aily 4031 Angleur, Belgium
[5] Physikalisch-Technische Bundesanstalt (PTB), Abbestr. 2-12, 10587 Berlin, Germany
[6] LPCE, UMR 6115 CNRS-Université d'Orléans, 3A Av. de la Recherche Scientifique, 45071 Orléans Cedex 2, France
[7] Royal Meteorological Institute of Belgium, Circular Avenue 3, 1180 Brussels, Belgium
[8] Belgian Institute for Space Aeronomy, Circular Avenue 3, 1180 Brussels, Belgium
[9] Solar Terrestrial Center of Excellence (STCE), Circular Avenue 3, 1180 Brussels, Belgium

Received 7 August 2009 / Accepted 25 October 2009

ABSTRACT

Aims. LYRA, the Large Yield Radiometer, is a vacuum ultraviolet (VUV) solar radiometer, planned to be launched in November 2009 on the European Space Agency PROBA2, the Project for On-Board Autonomy spacecraft.
Methods. The instrument was radiometrically calibrated in the radiometry laboratory of the Physikalisch-Technische Bundesanstalt (PTB) at the Berlin Electron Storage ring for SYnchroton radiation (BESSY II). The calibration was done using monochromatized synchrotron radiation at PTB's VUV and soft X-ray radiometry beamlines using reference detectors calibrated with the help of an electrical substitution radiometer as the primary detector standard.
Results. A total relative uncertainty of the radiometric calibration of the LYRA instrument between 1% and 11% was achieved. LYRA will provide irradiance data of the Sun in four UV passbands and with high temporal resolution down to 10 ms. The present state of the LYRA pre-flight calibration is presented as well as the expected instrument performance.

Key words. instrumentation: detectors – instrumentation: photometers – Sun: UV radiation

1. Introduction

LYRA, the Large Yield RAdiometer (Hochedez et al. 2006), is a solar vacuum ultraviolet (VUV) radiometer onboard PROBA2 (PRoject for On-Board Autonomy), a technologically oriented European Space Agency (ESA) micro-mission conceived for the purpose of demonstrating new technologies with prototype payloads. LYRA is designed and manufactured by a Belgian-Swiss-German consortium with additional international contributions from Japan, USA and Russia (see http://lyra.oma.be). LYRA will monitor the solar irradiance in four selected UV passbands simultaneously. These passbands have been chosen for their relevance to aeronomy, space weather and solar physics. Its four channels are labeled (1) the H I 121.6 nm Lyman-alpha line, (2) the 200–220 nm Herzberg continuum range, (3) the 17–80 nm aluminium filter range including the He II 30.4 nm line, and (4) the 6–20 nm zirconium filter range, where solar variability is highest. LYRA will be unique in adding the capability of fast measurements aiming at a highest possible cadence of 100 Hz, i.e., providing a set of measurements every 10 ms. LYRA measurements will provide the Aeronomy community with relevant solar irradiance observations and will reveal the sub-second structure of the solar flux for the first time. A main driver of the mission is the first-time use of novel diamond photodetectors in space. LYRA will be the first space assessment of a pioneering UV diamond detector program (see http://bold.oma.be). LYRA will be operated together with the extreme-ultraviolet telescope using new active pixel sensor (APS) technology – the Sun Watcher using APS and image Processing (SWAP) experiment (Berghmans et al. 2006). SWAP will provide images of the solar corona at a temperature of above one million degrees (Fe IX/X 17.4 nm emission line) at an improved image cadence typically one image every minute.

2. LYRA overview

2.1. Design

The dimensions of LYRA are 315 mm × 92.5 mm × 222 mm, and its weight is 3.533 kg. The detectors are grouped into three units (see Fig. 1), each containing four individual detection channels for each of the spectral bands mentioned above. Each detection channel consists of a cover mechanism, a collimator, a precision aperture, a spectral filter, a detector and two LED light sources. These LEDs, emitting at 375 and 470 nm wavelengths at room temperature, will help disentangle aging of the detectors from the filters (see Fig. 12). The three units are operated as redundant radiometers to maximize the accuracy and the reliability of the measurements. The two redundant groups of multiplexers/voltage-to-frequency converters (VFC) can be used

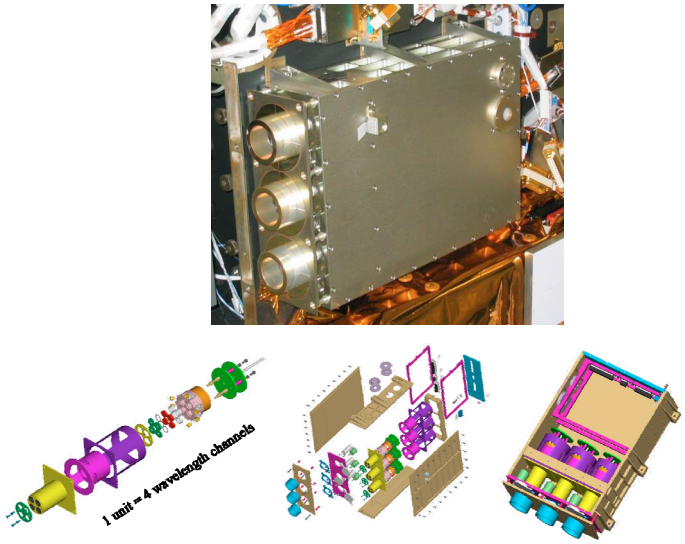

Fig. 1. Photograph of LYRA and an exploded view of one of the 3 redundant LYRA units. The total dimensions of LYRA are 315 mm × 92.5 mm × 222 mm, and its weight is 3.553 kg.

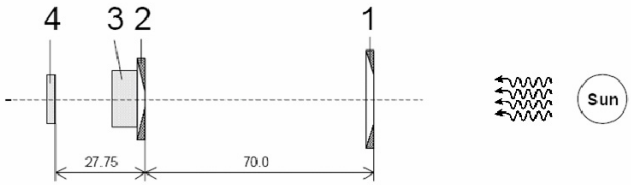

Fig. 2. Schematic representation of the optical path of a LYRA channel (not to scale) which consists of a view-limiting aperture (1), a precision aperture (2), an optical filter (3) and the detector (4).

to read one unit simultaneously to achieve a test of the VFC or two units (eight spectral channels) can be acquired in parallel to inter-calibrate the spectral channels. The selected filter-detector combinations representing the four UV passbands on the three redundant units will subsequently be called channels 1-1 to 3-4 (see Table 1).

Figure 2 shows the optical path of a LYRA channel. Given the geometry of the collimator, view-limiting apertures of 8 mm diameter, precision apertures of 3 mm diameter and detector sensitive area of 4.0 mm diameter, the field of view (FOV) is ±1° reduced by mounting tolerances to ±0.62°. Provisions have been taken for mounting tolerances, spacecraft off-points, and possible jitter. Note that there are no baffles between the view-limiting and the precision aperture. But after the precision aperture the four channels are totally separated and different tests in the optics laboratory showed that there is no need for stray light correction.

2.2. Cover mechanism

Each of the LYRA units is equipped with an individual cover mechanism, which provides a reduction of contamination during ground activities and a shutter mechanism for the filter radiometer. The design of the LYRA cover mechanism is shown in Fig. 3. The mechanism consists of a stepper motor procured from CDA Intercorp, a rotating cover, two position sensors and a launch lock device from Starsys Research. The stepper motor rotates the cover by 90° to open and close the optical path

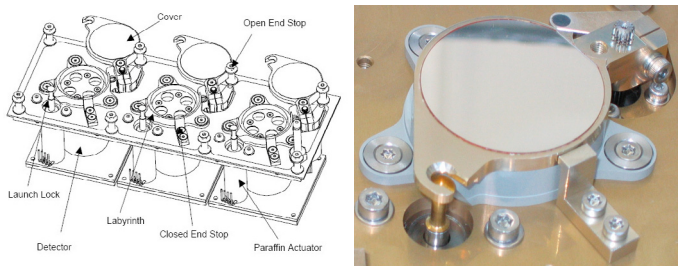

Fig. 3. Design and picture of the LYRA cover mechanism.

of LYRA instrument. Two hall sensors allow detection of fully open and closed position. A cover movement requires approximately 400 ms. The cover is manufactured of aluminum alloy 6082 and its Sun exposed surface is coated with a Back Surface Mirror (BSM) in order to reduce energy absorption during closed phases. An actuator locks the cover in closed position during launch. The implemented paraffin actuator allows a linear movement of the locking pin by approximately 10 mm. A heating element melts the paraffin, it expands during melting and thus the pin moves out. The needed power to be applied is in the order of 4.7 W for a period of 180 s. This is transformed into a gentle high force shaft extension of the piston. An internal spring returns the mechanism to its initial position when the current is turned off.

2.3. Contamination plan

At EUV wavelengths, molecular contamination on optical surfaces is an absorbing layer. Consequently to prevent contamination of optical surfaces, it is required that LYRA be continuously purged with nitrogen prior to launch and the cover always closed. The cover actually reduces the cleanliness requirements during the spacecraft tests activities, so that the contamination levels are acceptable. When during the tests the cover must be open, the environmental conditions are such that the cleanliness level can be met. This requires in general a controlled clean room area of class 10 000 if the instrument must stay open for more than one hour. It should be added that LYRA has the possibility to switch periodically heaters located close to the detectors and filters, in order to achieve a few degrees over temperature against the surrounding parts. Note that the photodetectors are operating close to the room temperature (between 20–30 °C) to avoid cold trapping. Once in flight, the LYRA instrument will open the entrance covers for a period venting of the optical compartment without UV light entering into the optical path. During orbital manoeuvres, the LYRA covers will be closed, in order to prevent contamination of the filters. The degradation of LYRA will be quantitatively accessible through the redundancy concept and the onboard LEDs.

3. LYRA calibrations

One scientific goal of LYRA is to improve the absolute accuracy of solar irradiance measurements, hence the need for subsystems and system calibration, on ground and in flight. The radiometric responsivity of each LYRA channel has to be determined over a wavelength range that is very large: from the soft X-ray (1 nm) to the near infrared (NIR) regime. First, subsystems (filters and detectors) were characterized for their UV responsivity, visible light blocking, background noise, dark current, linearity, and temporal stability within different wavelength

ranges. Second, the LYRA instrument was calibrated, channel per channel.

3.1. Calibration setup and measurements

The measurements were carried out by several teams at radiometric calibration facilities. PTB with its radiometry laboratory at the electron storage ring BESSY II provided the traceability to a primary detector standard. Calibration campaigns were conducted in 2005, 2006, and 2007. The synchrotron radiation calibration campaigns were carried out at the soft X-ray grazing incidence (GI) radiometry beamline (wavelength range 1 to 30 nm) and at the VUV normal incidence beamline (NI, 40 to 240 nm). Details of the description of the measuring stations can be found in Scholze et al. (2000) and Richter et al. (2003). The radiometric beamlines of PTB were operated with settings optimized for highest spectral purity of the monochromatized radiation. The relative contribution of all wavelengths to the detector wavelength range, the spectral impurities was kept below 1%. The relative standard uncertainty of the measurements was estimated to be better than a few percent. Individual measurements were repeated to check stability and reproducibility. For the longer wavelength range, monochromatic light was generated with a UV-enhanced 100 W deuterium lamp ($\lambda > 200$ nm), a double monochromator, and appropriate filters. For the low energy region ($\lambda > 350$ nm), the lamp was replaced by a tungsten halogen lamp or by different lasers with a beam homogeneity improved by an arrangement of pinhole and lenses. The intensity of the light could also be modulated by means of a mechanical chopper placed in front of the entrance slit. A schematic representation of the setup can be found in BenMoussa et al. (2004). Corrections for offset were applied. The estimated uncertainties are around 10% in the visible (VIS) and NIR region and roughly correspond to the size of the symbols used to plot data points.

3.2. Aperture area

The precision aperture (3.0 mm) of LYRA is not critical but its size must be carefully calibrated. After manufacturing, the apertures were sent to the Swiss Federal Office of Metrology and Accreditation (METAS) for calibration. The manufacturing tolerance of the precision apertures is H7 or $+10/-0$ μm in diameter. The inspection of roundness allows area calibration by diameter. As an example, the precision aperture area of channel 1-1 was measured as $A = 7.138 \pm 0.003$ mm^2 (with a coverage factor of $k = 2$ i.e. a level of confidence of 95%).

3.3. Filter transmittance

The optical filters were manufactured by Acton Research Corporation (ARC) for channels 1 and 2, i.e. Lyman-α and Herzberg, and by Luxel Corporation for the EUV and soft X-ray channels i.e. channels 3 and 4. All LYRA optical filters are mounted inside a 10 mm diameter ring with a maximal length of 7.5 mm. Filters were visually and optically checked before integration inside the LYRA heads, including individual transmittance measurements to show specific performance characteristics, i.e. bandwidth and light rejection. The filter and detector configuration for each channel are summarized in Table 1. Note that two stacked Lyman-α filters [XN+N] are used for channel [3-1] to improve the NUV-VIS-NIR rejection when using silicon (Si) AXUV photodetectors. Also the thickness of the Zr filters in channels [1-4] and [3-4] were increased to 300 nm when using Si photodetectors.

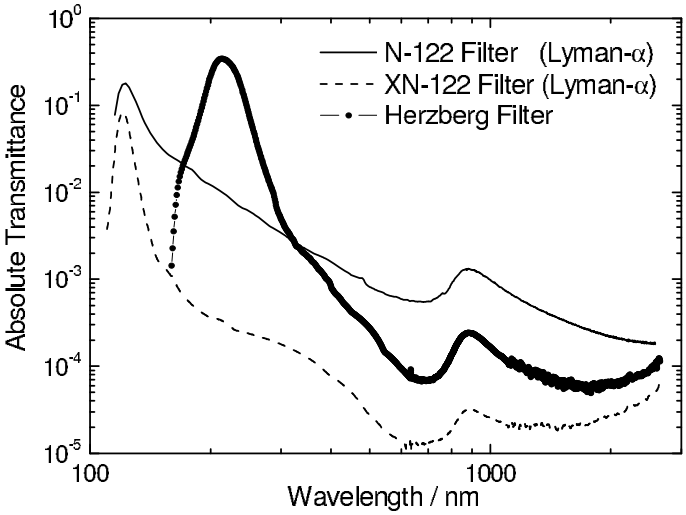

Fig. 4. Measured spectral transmittance of the Acton Research corp. filters: Lyman-α filters (N122, XN122) and 210-B Herzberg filter between 110 nm and 2600 nm.

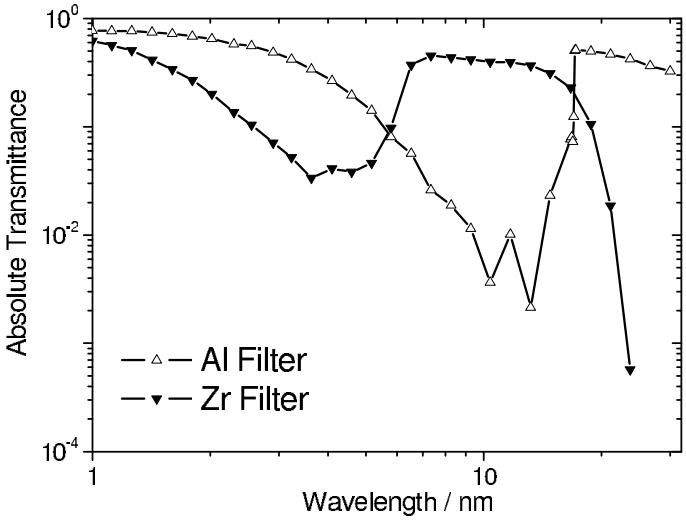

Fig. 5. Measured spectral transmittance of the Al (157.9 nm thick) and the Zr (141.3 nm thick) filters from Luxel corp. between 1 and 30 nm.

Figures 4 and 5 show the results of the spectral transmittance measurements carried out at different facilities, e.g., PTB/BESSY II, lasers and monochromatic light between 200–1100 nm, and Fourier Transform IR Spectrometer (FTIR) for wavelengths up to 2600 nm. It should be noted that within the uncertainties, the LYRA filters of the different units show the same transmittance curves, respectively.

3.4. Diamond photodetectors

For the LYRA project, two types of diamond detectors were developed: metal-semiconductor-metal (MSM) photoconductor and PIN photodiode detectors. Diamond detector structures were developed in a joint collaboration between IMO-IMOMEC in Belgium, NIMS in Japan, and Garching Analytics GmbH in Germany. Photographs of the diamond MSM and PIN detectors mounted inside their rectangular ceramic package are shown in Fig. 6. Device operation and fabrication procedure details are

Table 1. Selected configuration of LYRA channels.

ch.#	Filter label (thickness)	Bandwidth	Manufacturer	Detector
Unit 1				
1-1	Lyman α [XN]	120 nm to 123 nm	ARC	MSM12
1-2	Herzberg	200 nm to 220 nm	ARC	PIN10
1-3	Aluminium (158 nm)	17 nm to 80 nm	Luxel	MSM11
1-4	Zirconium (300 nm)	6 nm to 20 nm	Luxel	AXUV-20D
Unit 2				
2-1	Lyman α [XN]	120 nm to 123 nm	ARC	MSM21
2-2	Herzberg	200 nm to 220 nm	ARC	PIN11
2-3	Aluminium (158 nm)	17 nm to 80 nm	Luxel	MSM15
2-4	Zirconium (141 nm)	6 nm to 20 nm	Luxel	MSM19
Unit 3				
3-1	Lyman α [N+XN]	120 nm to 123 nm	ARC	AXUV-20A
3-2	Herzberg	200 nm to 220 nm	ARC	PIN12
3-3	Aluminium (158 nm)	17 nm to 80 nm	Luxel	AXUV-20B
3-4	Zirconium (300 nm)	6 nm to 20 nm	Luxel	AXUV-20C

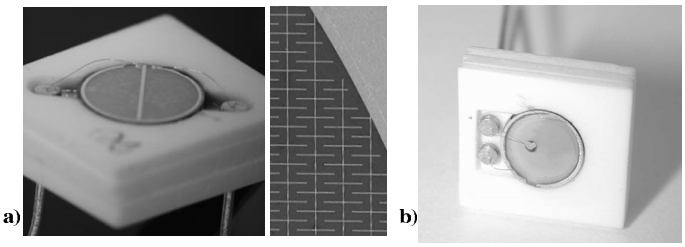

Fig. 6. Photograph of the diamond photodetectors **a)** MSM and detail of the Ti/Pt/Au contact structures; **b)** the PIN photodiode.

given elsewhere (BenMoussa et al. 2006a,b). Their particular advantage compared to Si detectors (AXUV from IRD) lies in their solar-blindness with an UV/VIS rejection ratio of at least four orders of magnitude. Indeed diamond is a wide bandgap semiconductor, which makes the sensors "solar-blind", i.e. insensitive to the solar spectrum below the Earth's atmosphere, at sea level, with a good UV/VIS rejection ratio. By using diamond detectors, the number of filters, blocking the unwanted visible radiation, can be reduced and the serious attenuation of the desired UV radiation can be minimized. Diamond exhibits several other superior properties compared to silicon. It has high charge carrier mobility at room temperature and a higher breakdown electric field, a low dielectric constant (thus low capacitance). The low intrinsic carrier density (smaller by seven orders of magnitude than silicon) makes cooling for noise reduction unnecessary. Its dense tetrahedral structure and stable covalent sp^3 bonding are the reasons for the expected radiation hardness of diamond detectors.

3.4.1. Dark current

The variation of the dark current with temperature was investigated in pre-flight tests. Thermal cycles were performed between −40 °C and +60 °C. As an example, the signal of the MSM photodetector shows a sub-pA variation following the temperature evolution (0.1 °C steps) with a small hysteresis when repeated. The performance of the detector does not change after the thermal cycling. Indeed, the performance of the MSM photodetectors depends significantly on the surface properties of the active layer (diamond), on the applied voltage, and on the geometrical design, especially the distance between electrodes. The MSM detector channels show negligibly small (few pA) dark current over the area of the entire detector at room temperature. The PIN detector channels (channel *-2) are faster devices due to their low capacitance. Diamond PIN photodiodes typically have no dark currents (background detrapping 10^{-14} A). Note that the PIN photodiodes (both diamond and Si-AXUV) are operated in a photovoltaic mode (unbiased) while the diamond MSM operational voltage is 5 V bias.

3.4.2. Photodetectors spectral responsivity

The typical absolute spectral responsivity of the LYRA photodetectors is shown in Fig. 7. The data from 210 nm to 1000 nm (measured on a relative scale) were matched to the absolute data from PTB/BESSY II (1 nm to 240 nm). The responsivities of the diamond photodetectors (MSM and PIN) show the diamond band edge to be around 225 nm and display a UV/VIS rejection ratio (200 nm /500 nm) of more than 4 orders of magnitude. The responsivity of the diamond PIN photodiode (used only for the Herzberg channels) decreases dramatically below 180 nm due to the absorption of the 300 nm thick n-type layer associated with the abrupt drop of the diamond penetration depth which is about 20 nm at 170 nm wavelength. Thus, electron-hole pairs are created very close to the surface and recombine before reaching the depletion region. The MSM diamond detector sensitivity covers the spectral range going from 1 nm up to 220 nm and the Si AXUV detectors from 1 nm to 1100 nm.

3.5. LYRA calibration results

3.5.1. Absolute spectral responsivity

We report on the calibration results needed for future scientific analysis. This includes in-depth characterization and understanding of the global LYRA instrument response. Figures 8 show the spectral responsivity values (in A/W) for the LYRA selected filter-detector combinations of its four channels. For clarity we did not plot the corresponding error bars. A compilation of their contributions to the measurement uncertainties in the spectral responsivity is given in Scholze et al. (2003) and Richter et al. (2003). The observed differences in the absolute combined responsivity in Figs. 8 (see top panels) are mainly due to the discrepancies between the various prototype diamond flight sensors. These diamond photodetectors prove their general suitability for space solar observations, nevertheless diamond must still be acknowledged as relying on new/emerging technology.

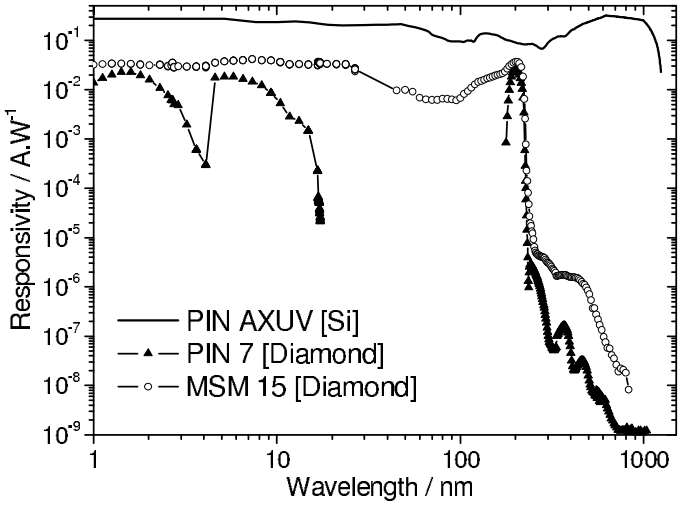

Fig. 7. Spectral response of a typical Si AXUV n-on-p photodiode (unbiased), diamond PIN photodiode (unbiased) and diamond MSM (under 5 V bias) between 1 nm and 1000 nm.

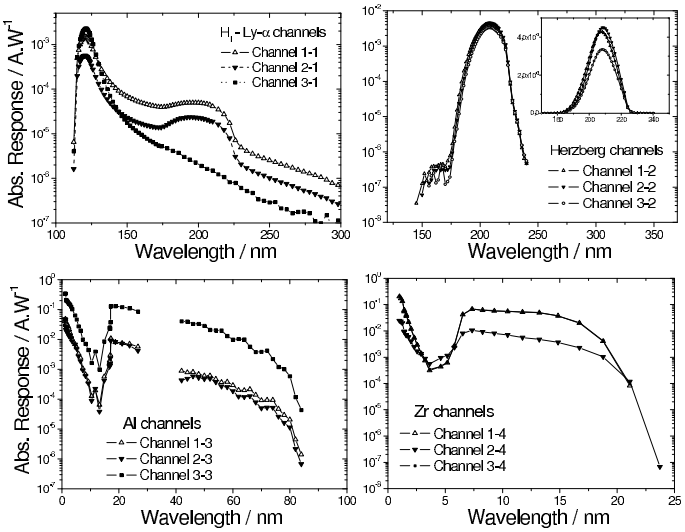

Fig. 8. *Top left*: absolute responsivity of the Lyman-α channels between 110 nm and 300 nm wavelength. *Top right*: absolute responsivity of the Herzberg channels between 150 nm and 240 nm wavelength. The inset shows a close-up view on linear scale. *Bottom left*: absolute responsivity of the Al channels between 1 nm and 84 nm wavelength. *Bottom right*: absolute responsivity of the Zr channels between 1 nm and 24 nm wavelength.

Further improvements of their performance characteristics are still needed.

3.5.2. Uniformity of the photoresponse (flat-field)

The spatial homogeneity varies from detector to detector and necessitates the need for calibrating each channel's detector over a wide wavelength range. The detector calibration chambers at the beamlines of PTB at BESSY II allow the sample to be moved along three axes relative to the beam axis in ultra-high vacuum. This makes it possible to raster scan the sample area with the incoming beam. Toggling between test and reference detectors is possible as well. The spot size of the raster beam is approximately 0.3 mm × 0.3 mm (*FWHM*) in the GI beamline, and 0.6 mm × 0.6 mm (*FWHM*) in the NI beamline,

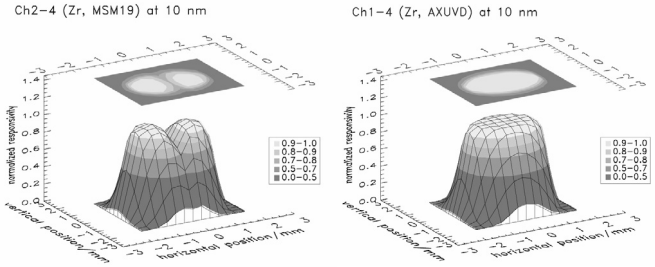

Fig. 9. Homogeneity of the responsivity (3-D representation) of channel 2-4 (MSM diamond photodetector, *left panel*) and channel 1-4 (Si-AXUV, *right panel*) at 10 nm wavelength.

depending slightly on the chosen wavelength. Individual measurements were repeated to check stability and reproducibility. The beamline power was readjusted between scans to better conform to detector sensitivities. The relative responsivity maps were built by normalizing the current to its maximum value to help comparison. Figure 9 shows a 3-dimensional representation of the LYRA channel raster scans at 10 nm. The flat field quality is wavelength dependent. As we can see, the homogeneity of the MSM diamond photodetector (left panel) seems to be moderate. The sharp dip in responsivity (40 to 50% deviation) observed at the centre of the MSM channels is related to the geometrical arrangement of the contact electrodes (cf. Fig. 6a) and the width of the raster beam (convolution). The shadowing of the active area by the interdigitated contacts is the main drawback of those particular MSM detectors and results in a significant efficiency reduction. New device architectures are under development to maximize the fill factor and increase the homogeneity of the MSM photodetectors (BenMoussa et al. 2008) but they will not fly on LYRA.

Note that the knowledge of the flat field is used to correct the measured responsivity of each LYRA channel. Taking into account that the beam at the PTB/BESSYII covered only a subarea in the centre of the detector, the expected effect was simulated and responsivity values were accordingly modified, between 0% and –28% (Dammasch 2008). Knowledge of the flat field will also be necessary to correct for off-pointing effects when the circular image of the Sun through the 3 mm precision aperture will move outward from the center of the detector. Pre-flight simulations will be tested and updated, in order to construct a table that delivers correction factors. Simulations show that ±1° off-pointing leads to approximately 20–25% reduction from the nominal response (see Dammasch 2006). Off-pointing on the order of the nominal jitter of PROBA2 (5 arcmin) leads to fluctuations of approximately ±1% around the nominal response. Note that off-pointing on the order of the offset between SWAP and LYRA will therefore not be detectable.

3.5.3. Linearity vs. photon flux

The linearity of the different LYRA channels has been investigated over 3 orders of magnitude (from 1 nW to 1 μW) at PTB/BESSY II, using different aperture stops to reduce the radiant power to lowest measurable values (minimum 1% of the full beam power), or by varying the exit slit of the monochromator. The absolute input radiant power was determined for each aperture by direct comparison with a calibrated Si reference photodiode. A power law:

$$I = a\, P^b \qquad (1)$$

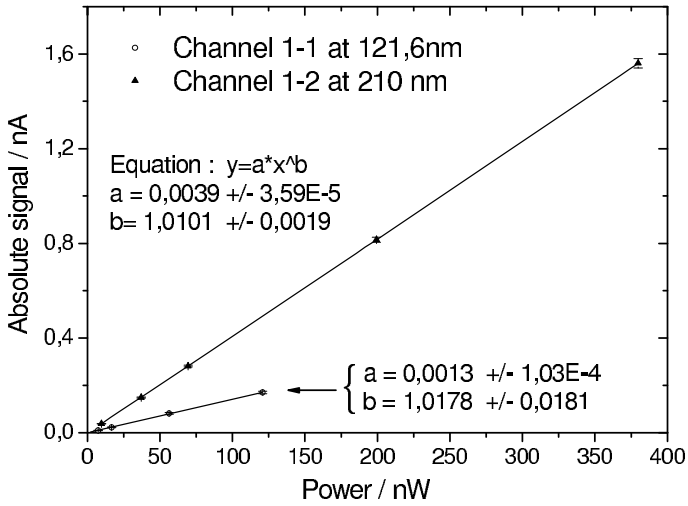

Fig. 10. Flux linearity of LYRA channels 1-1 and 1-2 (photocurrent versus incident power) at 121.6 nm and 210 nm respectively, with the fitted function (see Eq. (1)).

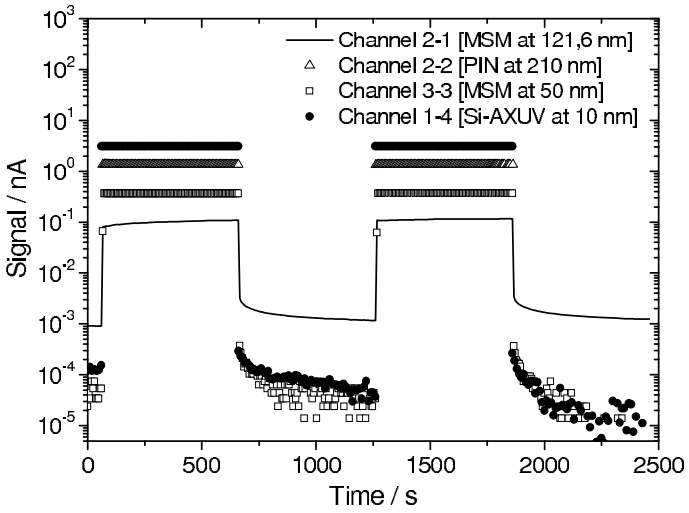

Fig. 11. Signal current (log scale) as a function of time for LYRA detectors at different wavelengths.

Table 2. Linearity fit parameters and their quality ($b > 1$ denotes super-linear and $b < 1$ sub-linear behavior).

ch.#	detector	Measurement, λ	Parameter b (±uncertainty)
Unit 1			
1-1	MSM12	NI 121.6 nm	1.018 (0.018)
1-2	PIN10	NI 210 nm	1.010 (0.002)
1-3	MSM11	NI 50 nm	1.131 (0.046)
1-3	MSM11	GI 18 nm	1.179 (0.007)
1-4	AXUV-20D	GI 10 nm	1.018 (0.002)
Unit 2			
2-1	MSM21	NI 121.6 nm	1.033 (0.010)
2-2	PIN11	NI 210 nm	1.006 (0.004)
2-3	MSM15	NI 50 nm	1.022 (0.038)
2-3	MSM15	GI 18 nm	1.090 (0.005)
2-4	MSM19	GI 10 nm	1.086 (0.009)
Unit 3			
3-1	AXUV-20A	NI 121.6 nm	1.039 (0.010)
3-2	PIN12	NI 210 nm	0.989 (0.005)
3-3	AXUV-20B	NI 50 nm	0.978 (0.011)
3-3	AXUV-20B	GI 18 nm	1.001 (0.001)
3-4	AXUV-20C	GI 10 nm	0.998 (0.002)

was used to fit the data where I is the signal current and P the incident beam power. As shown in Fig. 10, the fitted parameters for channel 1-1 are $a = (0.0013 \pm 0.0001)$ A/W and $b = (1.0178 \pm 0.0181)$, which implies a linear (within uncertainties) dependence of the output signal on the incident power ($b < 1$ would denote sub-linear photoresponse). For channel 1-2, a slightly super-linear dependence with $a = (0.0039 \pm 0.00004)$ A/W and $b = (1.0101 \pm 0.0019)$ is obtained at 210 nm wavelength. Table 2 shows the behavior dominating fit parameter b for all LYRA channels.

3.5.4. Signal stability

The stability of the output signal under irradiation over prolonged periods is an important mission goal for a radiometer. The redundancy concept (although the units are not strictly identical) completes the strategy to stability monitoring. One unit will be used continuously, another one on a weekly basis, while the last one will remain closed most of the time and will only be used a few times during the mission. In this way, the radiometric evolution of the sensors and filters will be assessed. Furthermore, the responsivity of the detectors, i.e. the sub-gap photoresponse for diamond, will be monitored by on-board light sources (LEDs) in order to distinguish a detector's drift from degradations of the filters. The LEDs (VIS LEDs emitting at 470 nm and NUV LEDs emitting at 375 nm) are situated between the filter and detector, but outside the optical path from the sun viewed by the detector through a precision hole (see in Fig. 12). Thus the LEDs will monitor only the degradation of the detector (not the optical filters).

Note that reliability measurements on the LEDs have been carried out. In particular the 12 NUV and 12 VIS LEDs selected for LYRA have been measured between –40 and +60 °C. At each measurement point, a diode emission spectra has been taken. From the measured spectra it is clear that the emission intensity is strongly temperature dependent. Also the LED emission maximum is shifted with the temperature. The temperature changes from –40 to +60 °C cause a shift of typically 5 nm, for both NUV and VIS LEDs. This shift is from 373 to 378 nm for NUV diodes and from 468 to 473 nm for the VIS diodes. The LED calibration has been carried out in the LYRA head with mounted detectors. There were several hours of LED tests performed with the PTB-BESSY II beamlines. For the resulting data, see Dammasch (2007). Note also that the LEDs can be operated in pulse mode (10 Hz max.) to avoid an increase of its junction temperature.

Similarly as for the linearity, the signal stability at room temperature was measured at five wavelengths: 121.6 nm for the Lyman-α channels, 210 nm for the Herzberg channels, 50 nm and 18 nm for the Al channels, and 10 nm for the Zr channels. In order to characterize the temporal response of the detectors, the beamline shutter was opened and closed approximately every 600 s. The data are corrected for the small decline (1%) of the current of the synchrotron storage ring during the time period of each measurement. Figure 11 shows the total signal as a function of time, for different LYRA channels using diamond MSM, PIN and Si AXUV detectors on the same time scale, in order to demonstrate the differences in temporal behavior. For additional information see BenMoussa et al. (2006b) and BenMoussa (2006a,b).

All LYRA channels show a good stability on a wide temporal range with a small room-temperature dark current. At 121.6 nm (Lyman-α line), the MSM detectors appear to be less stable.

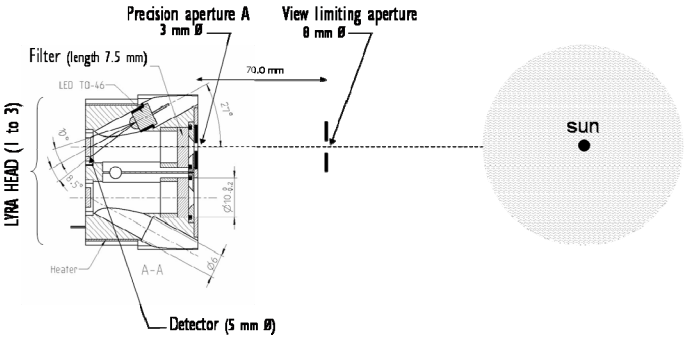

Fig. 12. Schematic representation of a LYRA unit (head) with its detectors, filters, LEDs and its two apertures (not to scale).

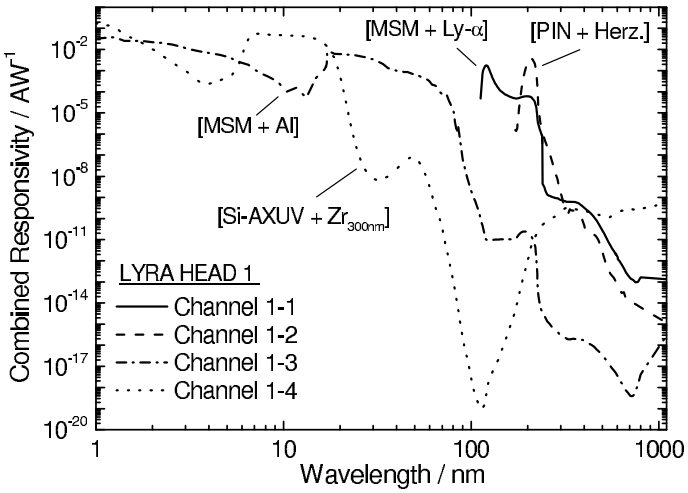

Fig. 13. Combined simulated spectral responsivity [detector + filter] for LYRA unit 1 between 1 and 1100 nm.

Indeed the penetration depth has extremely small values, of the order of a few nanometers. The photons are, thus, being absorbed in the first atomic layers, leading to carrier recombination in the surface and consequently to a reduction of the stability. The time to reach a stable signal varied depending on the irradiation power. During the first minutes approximately, the signal increases progressively and then tends to be stable with a signal drift of less than 1%. One possible explanation for the initial increase of the signal is attributed to the filling of localized empty states (due to surface defects) until no more electron-hole pairs can be trapped. When the traps are filled, the signal remains stable. During prolonged duration without irradiation, the progressive return to an equilibrium condition with the release of trapped charge (detrapping) of different defect levels in the bandgap results in the slow decrease of the dark current.

4. Radiometric model

A radiometric model based on the solar spectral irradiance, transmittance of the filters, and detectors' responsivity is used to determine the anticipated photocurrents and their spectral purity (see http://lyra.oma.be). Based on these simulations, twelve channel configurations for the three LYRA units were selected and equipped as summarized in Table 1.

4.1. Principle

Photons from the sun with the spectral irradiance $E_\lambda(\lambda)$ enter the LYRA instrument through a circular aperture A of 3 mm in diameter, pass one set of filters of a certain (dimensionless) transmittance $F(\lambda)$, and are converted to an electric current by a detector with a certain spectral responsivity $D(\lambda)$, measured in A/W. The aperture A determines the amount of optical power incident upon the detector from the sun (see Fig. 12). Here, the diffraction effect can be ignored, since the aperture is large compared to the wavelength of light being used, and the detector has a diameter sufficient to intercept all the radiation exiting through the aperture. With the integration time T, the expected photocurrent is then,

$$i = \frac{A}{T} \int_t \int_\lambda E(\lambda, t)\, F(\lambda)\, D(\lambda)\, \mathrm{d}\lambda\, \mathrm{d}t, \qquad (2)$$

where $i = i_\mathrm{s} + i_\mathrm{d}$ with i_s being the signal from the solar spectra and i_d the dark current contribution.

4.2. Simulations

Some approximations such as extrapolations towards the EUV and the NIR of the Al and Zr filters transmittance were carried out where the rejection of light was too high to be adequately measured. In the EUV, the filter transmittance was modelled and matched to the absolute data from PTB/BESSY II using the data of the Center for X-Ray Optics (CXRO) at the Lawrence Berkeley National Laboratory (LBNL), available at http://www-cxro.lbl.gov/. A Jobin-Yvon software was used to determine the transmittance of the Al and Zr filters in the NUV and VIS range. The oxide thicknesses of the metallic filters were taken into account by fitting the absolute transmittance between 1 nm and 30 nm. The 70-lines-per-inch nickel mesh used to support the Al and Zr filters transmits about 82%. Theoretical calculations of long-wavelength extensions were corrected by on-ground measurements performed at PMOD/WRC in Davos. As a result, Fig. 13 shows the combined spectral responsivity of the four LYRA channels of unit 1 between 1 and 1100 nm.

To determine the anticipated photocurrents, the spectral responsivities were multiplied with solar sample spectra originating from instruments already in space, namely TIMED/SEE (http://www.timed.jhuapl.edu/WWW/index.php) for shorter wavelengths, suitable for LYRA channels 3 and 4, and SORCE (http://lasp.colorado.edu/sorce/index.htm) for longer wavelengths, suitable for LYRA channels 1 and 2. By now, these instruments have covered several years of the solar cycle, thus spectra could be selected representing solar minimum and maximum conditions, as well as situations of various solar activities such as pre-flare and post-flare conditions. Seven sample spectra were tested against twelve responsivity curves (see Dammasch 2009a). Figure 14 shows an example for the LYRA radiometric model simulations.

As can be seen from Figs. 14 and 15, LYRA channels are not merely responding in their nominal spectral intervals, but also receive contaminations from other ranges. The purity of a channel is defined as the ratio of the flux in the nominal wavelength range (LYRA bandwidth channels) to the total output signal. Table 3 shows the total signals and purities as expected according to the radiometric model described in the section above. Listed are the total values estimated for the minimal and maximal solar spectra as observed by the TIMED/SEE and SORCE instruments, namely, a minimum solar spectrum of 29 June 2008, and a maximum (flare) spectrum of 28 October 2003.

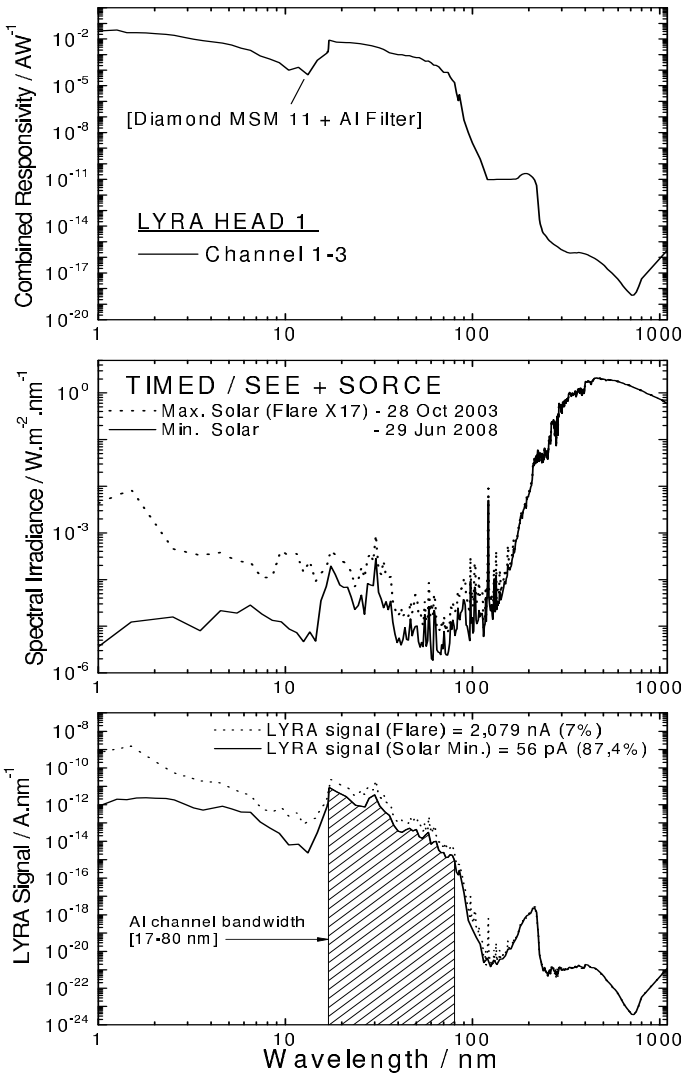

Fig. 14. Examples for LYRA radiometric model simulations. *From top to bottom*: channel 1-3's responsivity curve (MSM detector + Al filter), the solar spectrum (maximum and minimum solar spectrum from 2003 and 2008, respectively), and the product of both; the integral of the last curve estimates the total output signal of the LYRA channel, when multiplied with the area of the precision aperture A.

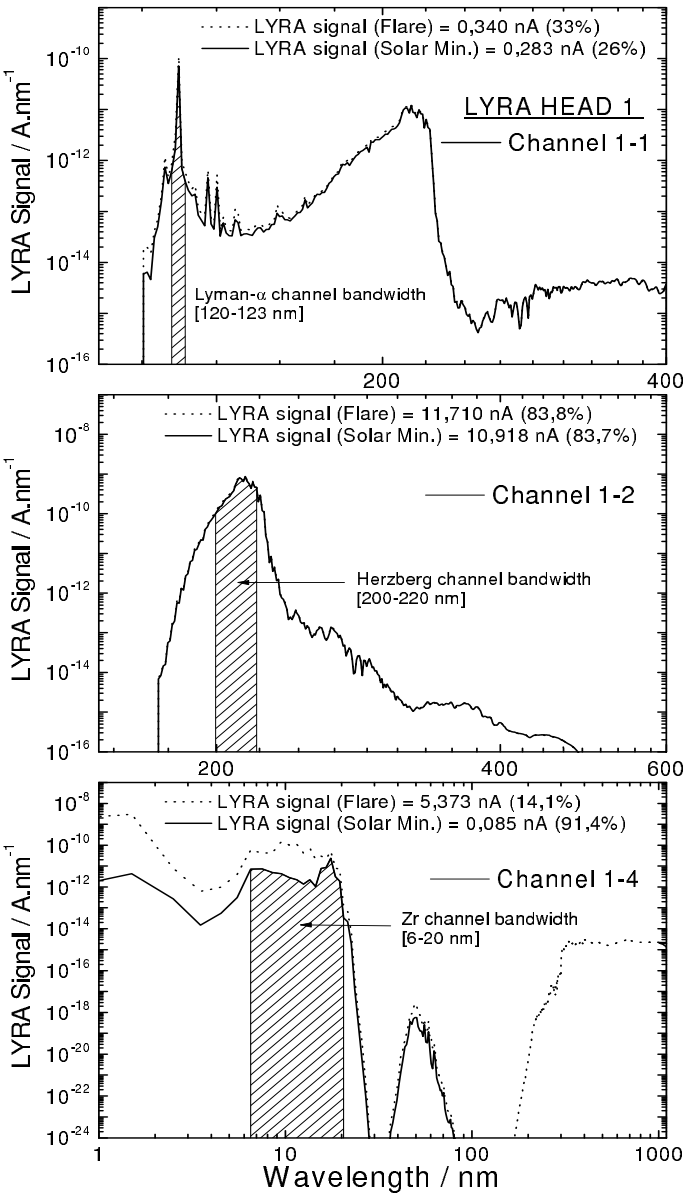

Fig. 15. Examples of LYRA radiometric model simulations for channels 1-1, 1-2 and 1-4.

As a result, Lyra will measure an estimated signal between 0.01 to 17 nA. The high sensitivity of the MSM detectors at around 200–220 nm results in a portion of the solar continuum to the Lyman-α channel signal and thus in a lower signal purity, around 25% compared to the 32% when using Si-AXUV photodetector (see channel 3-1). Note that the purity of the Lyman-α channels increases slightly at solar maximum. Indeed the 200–220 nm contribution is quite stable while the Lyman-α line shows a higher variability between the solar minimum and maximum. For the Herzberg channels, the expected signal and purities are high and stable. The Herzberg channel is well defined by its bandwidth with a low contamination from the other wavelengths. It shows a purity of about 84% under all solar spectrum conditions. Note that channels 1 and 2 display smaller solar signal variability as compared to the channels 3 and 4. The advantage of the first two channels is that their purity appears to be rather stable. On the contrary, the solar EUV radiation is highly variable (Woods & Chamberlin 2009; Woods et al. 2005a,b). Al and Zr channels display extreme variability with the solar conditions, as purity abruptly decreases when strong contamination from the soft X-ray range begins to dominate the signal in the case of high flux. One of the advantages of these two channels is that, although their purity is highly dependent on the incoming signal, additional information may be gained by a clever signal separation (Dammasch 2009b). As soon as the pure signal of the channels is determined, the relationship to the respective solar irradiance appears quite straightforward according to the radiometric model simulations. Another advantage of the latter two LYRA channels (*-3 and *-4) is the fact that they have a small overlap in responsivity around 17 nm, which is also the interval in which SWAP will observe the Sun.

4.3. LYRA uncertainty budget

The uncertainties for each LYRA channel are estimated taking into consideration possible uncertainties from responsivity measurements, extrapolations, and small fluctuations of the room temperature. According to Eq. (2), the mean spectral irradiance

Table 3. Example of the expected LYRA total output signals (nA) and purities (%) between brackets. Since not the entire IR spectrum is taken into account, these values rather represent a lower limit.

ch.#	Filter label	Bandwidth, nm	detector	Min. Signal (pur.)	Max. Signal (pur.)	Max. Signal /Min. Signal
Unit 1						
1-1	Lyman-α [XN]	120-123	MSM12	0.283 (26%)	0.340 (33%)	1.20
1-2	Herzberg	200-220	PIN10	10.918 (83.7%)	11.710 (83.8%)	1.07
1-3	Aluminium	17-80	MSM11	0.054 (86.7%)	2.079 (7.0%)	38.50
1-4	Zirconium	6-20	AXUV-20D	0.085 (91.4%)	5.373 (14.1%)	63.21
Unit 2						
2-1	Lyman-α [XN]	120-123	MSM21	0.100 (25.7%)	0.119 (32.8%)	1.19
2-2	Herzberg	200-220	PIN11	11.690 (83.8%)	12.512 (83.9%)	1.07
2-3	Aluminium	17-80	MSM15	0.049 (88.8%)	1.745 (7.8%)	35.61
2-4	Zirconium	6-20	MSM19	0.012 (86.1%)	0.787 (12.5%)	65.58
Unit 3						
3-1	Lyman-α [N+XN]	120-123	AXUV-20A	0.269 (32.5%)	0.317 (42.1%)	1.18
3-2	Herzberg	200-220	PIN12	9.389 (83.5%)	10.055 (83.6%)	1.07
3-3	Aluminium	17-80	AXUV-20B	0.907 (91.8%)	16.701 (16.1%)	18.41
3-4	Zirconium	6-20	AXUV-20C	0.087 (89.4%)	5.375 (14.1%)	61.78

Table 4. Example of the LYRA total uncertainty budget with 1s integration time ($\Delta T/T = \pm 7510^{-6}$) at solar minimum (spectrum of 29 June 2008). $\overline{\Delta E}/\overline{E}$ is the relative uncertainty of the LYRA instrument.

ch.#	$\Delta i/i \times 10^{-4}$	$\Delta A/A \times 10^{-4}$	$\Delta \int FD / \int FD \times 10^{-2}$	$\overline{\Delta E}/\overline{E} \times 10^{-2}$
Unit 1				
1-1	2.8	4.2	9.69	±9.77
1-2	0.1	4.2	5.88	±5.94
1-3	1.1	4.2	1.02	±1.08
1-4	0.7	5.6	1.00	±1.06
Unit 2				
2-1	0.1	5.6	11.49	±11.56
2-2	0.1	7.1	5.04	±5.12
2-3	1.3	5.6	1.22	±1.29
2-4	0.5	4.1	1.00	±1.05
Unit 3				
3-1	0.1	7.0	4.17	±4.24
3-2	0.1	5.6	3.17	±3.23
3-3	0.6	7.0	1.50	±1.59
3-4	0.7	7.1	1.00	±1.08

$\bar{E}_\lambda$ at the respective channel wavelength may be approximated by:

$$\bar{E}_\lambda = \frac{i}{A \int_\lambda F(\lambda)\, D(\lambda)\, \mathrm{d}\lambda} \cdot \tag{3}$$

All the relative uncertainties (uncorrelated) are evaluated for producing the LYRA standard uncertainty, as follows:

$$\frac{\overline{\Delta E}}{\overline{E}} \cong \frac{\Delta i}{i} + \frac{\Delta A}{A} + \frac{\Delta \int_\lambda F\, D\, \mathrm{d}\lambda}{\int_\lambda F\, D\, \mathrm{d}\lambda}, \tag{4}$$

with $i = i_\mathrm{s} + i_\mathrm{d}$ and $\Delta i = \Delta i_\mathrm{s} + \Delta i_\mathrm{d}$.

Note that the dark current (i_d) is measured with the cover closed before and after the signal acquisition with the same integration time. It is then substracted from the integrated signal to calculate i_s. The uncertainty on the integrated signal (i) is evaluated using three levels of a reference calibration voltage. Indeed the voltage-to-frequency converters (VFC) are not perfectly linear. To correct the measured values, three calibration voltages (0 V, 2.5 V, 5 V) are used. After the measurements, a polynomial fit (second order) can be applied to correct the measured values, if necessary. Note that a small offset is integrated, in order that 0 V input does not correspond to 0 Hz output. The VFC's are set to 5.635 V full-scale input, which equals to 1.2288 MHz. To convert the voltage to current, an uncertainty on the measuring gain resistor R and on the VFC offset are taken into account.

The LYRA integration time is generated with a 4.9152 MHz quartz crystal with a temporal resolution of 0.2 μs. The relative uncertainty of the quartz is ±(50 + 25) ppm for stability and tolerance of the frequency, which corresponds to a maximal uncertainty between two integration times of 1.5 ms (worst case) at 10 s and below 1.5 μs for the 10 ms integration time. The contributions to the measurement uncertainties of the filter-detector responsivities are given in Scholze et al. (2000); Richter et al. (2003). In addition, a relative uncertainty of 5% was applied to the detector photoresponse measured between 200 nm and 1100 nm, and 10% on the filter transmittance when extrapolated or measured above 240 nm. As an example, the relative uncertainty for each channel is reported in Table 4 with the expected output signals at solar minimum (spectrum of 29 June 2008).

5. Conclusions

LYRA is exceptional in several respects. It is the first time UV diamond detectors are going to be used in space, and particularly

for solar physics. They offer new potential to the future solar observation missions. The high cadence rate and low measurement uncertainty attainable by LYRA stems from them, and they promise radiation hardness. Additionally, LYRA profits from a redundancy design for tracking instrument degradation, LED light sources for in-flight monitoring, calibrations traceable to synchrotron source standards, and scientific synergies with SWAP, the sister solar instrument on board the PROBA2 satellite. For the calibration of LYRA, the responsivity, linearity, stability and homogeneity have been measured before final integration on the PROBA2 platform. The responsivity has been calibrated thoroughly in the wavelength range from 1 nm to 240 nm. LYRA channels show a high response for short wavelengths and a good NUV/VIS/IR rejection due to the combination of diamond photodetectors and optical filters. In the wavelength range of interest, LYRA channels are reasonably homogenous, linear, and stable under irradiation with a negligible dark current drift. A calibration software based on a radiometric model is used to determine spectral purity of the individual observation channels in dependence of the solar activity. These calibration functions will be tested in the commissioning phase and will be permanently updated to account for observed degradation and incorporate the results of cross-calibration among LYRA units and with other instruments.

Acknowledgements. The authors acknowledge the support from the Belgian Federal Science Policy Office through the ESA-PRODEX programme, the Max-Planck-Institut für Sonnensystemforschung and ISSI, Bern, funding of SCSL.

References

BenMoussa, A. 2006a, Pre-Analysis Report – Final calibration GI beamline (1–30 nm) – PROBA2/LYRA, Tech. Rep., Royal Observatory of Belgium
BenMoussa, A. 2006b, Pre-Analysis Report – Final calibration NI beamline (40–240 nm) – PROBA2/LYRA, Tech. Rep., Royal Observatory of Belgium
BenMoussa, A., Schühle, U., Haenen, K., et al. 2004, Physica Status Solidi Applied Research, 201, 2536
BenMoussa, A., Schühle, U., Scholze, F., et al. 2006a, Measurement Science and Technology, 17, 913
BenMoussa, A., Theissen, A., Scholze, F., et al. 2006b, Nucl. Instr. Meth. Phys. Res. A, 568, 398
BenMoussa, A., Soltani, A., Haenen, K., et al. 2008, Semiconductor Science Technology, 23, 035026
Berghmans, D., Hochedez, J. F., Defise, J. M., et al. 2006, Adv. Space Res., 38, 1807
Dammasch, I. 2006, LYRA Flatfield Software: Relative Output as Function of Pointing, Tech. Rep., Royal Observatory of Belgium
Dammasch, I. 2007, LYRA Dark Current and LED Measurements, Tech. Rep., Royal Observatory of Belgium
Dammasch, I. 2008, LYRA Responsivity: Update, Tech. Rep., Royal Observatory of Belgium
Dammasch, I. 2009a, LYRA Calibration Methods: New channels, Tech. Rep., Royal Observatory of Belgium
Dammasch, I. 2009b, LYRA Output: Expected Variations, Tech. Rep., Royal Observatory of Belgium
Hochedez, J.-F., Schmutz, W., Stockman, Y., et al. 2006, Adv. Space Res., 37, 303
Richter, M., Hollandt, J., Kroth, U., et al. 2003, Metrologia, 40, 107
Scholze, F., Beckhoff, B., Brandt, G., et al. 2000, in SPIE Conf. Ser. 4146, ed. W. M. Kaiser & R. H. Stulen, 72
Scholze, F., Tummler, J., & Ulm, G. 2003, Metrologia, 40, S224
Woods, T. N., & Chamberlin, P. C. 2009, Adv. Space Res., 43, 349
Woods, T. N., Eparvier, F. G., Bailey, S. M., et al. 2005a, J. Geophys. Res. (Space Phys.), 110, 1312
Woods, T. N., Rottman, G., & Vest, R. 2005b, Sol. Phys., 230, 345